SAR Image Denoising via Clustering-Based Principal Component Analysis

Linlin Xu, *Graduate Student Member, IEEE*, Jonathan Li, *Senior Member, IEEE*, Yuanming Shu, and Junhuan Peng

***Abstract*—The combination of nonlocal grouping and transformed domain filtering has led to the state-of-the-art denoising techniques. In this paper, we extend this line of study to the denoising of synthetic aperture radar (SAR) images based on clustering the noisy image into disjoint local regions with similar spatial structure and denoising each region by the linear minimum mean-square error (LMMSE) filtering in principal component analysis (PCA) domain. Both clustering and denoising are performed on image patches. For clustering, to reduce dimensionality and resist the influence of noise, several leading principal components identified by the minimum description length criterion are used to feed the K-means clustering algorithm. For denoising, to avoid the limitations of the homomorphic approach, we build our denoising scheme on additive signal-dependent noise model and derive a PCA-based LMMSE denoising model for multiplicative noise. Denoised patches of all clusters are finally used to reconstruct the noise-free image. The experiments demonstrate that the proposed algorithm achieved better performance than the referenced state-of-the-art methods in terms of both noise reduction and image detail preservation.**

***Index Terms*—Clustering, denoising, linear minimum mean-square error (LMMSE), minimum description length (MDL), principal component analysis (PCA), speckle noise, synthetic aperture radar (SAR).**

I. Introduction

SYNTHETIC aperture radar (SAR), as a coherent imaging system, is inherently suffering from speckle noise, which has a granular appearance and greatly impedes automatic image processing and visual interpretation. Although multilook averaging is a common way to suppress speckle noise at the cost of reduced spatial resolution, it is more favorable to develop suitable filtering techniques. Although classical filters, such as Lee filter [1], Frost filter [2], and Kuan filter [3], which denoise SAR images in spatial domain by recalculating the center pixels of the filtering windows based on the local scene heterogeneity, work well in stationary image area, they tend to either preserve speckle noise or erase a weak scene signal at heterogeneous areas, e.g., texture area, boundary, line, or point targets. In order to better preserve image edges, Yu and Acton in [4] designed a speckle reduction anisotropic diffusion (SRAD) method which can be treated as an edge-sensitive version of the classical filters. The performance of the gamma MAP filter [5], which denoises the SAR image via maximum *a posteriori* criteria, depends highly on whether the imposed gamma distribution can accurately describe the SAR image.

Instead of denoising in spatial domain, it has been proved more efficient to perform the task in transformed domain where the signal and noise are easier to separate. The wavelet techniques assume that noise mainly exists on the high-frequency wavelet components and thus can be removed by filtering the wavelet coefficients in transformed domain. This idea has proved great success to denoise additive white Gaussian noise (AWGN). To adapt wavelet for SAR denoising, many techniques adopted the homomorphic approach where speckle noise subject to log-transformation is treated as AWGN and denoised in wavelet domain by thresholding [6], [7] or modeling [8]–[10] the wavelet coefficients. However, since the performance of denoising is very sensitive to logarithmic operation that tends to distort the radiometric properties of the SAR image, techniques based on additive signal-dependent noise (ASDN) model were developed in [11]–[14].

Although wavelet-based denoising methods have proved better efficiency than classical filters, limitations reside in the inadequate representation of various local spatial structures in images using the fixed wavelet bases [15]–[17]. On the other hand, locally learned principal component analysis (PCA) bases, a series of mutually orthogonal directions with sequentially largest variances, have shown better capability of representing structural features, e.g., image edges and texture. In PCA domain, the scene signal is mostly captured by several leading principal components (PCs), while the last few components with low variances are mainly due to noise. The denoising of AWGN has been achieved by filtering the PCs through linear minimum mean-square error (LMMSE). Examples include the adaptive PCA denoising scheme proposed by Muresan and Parks [15] and local pixel grouping PCA (LPG-PCA) algorithm proposed by Zhang *et al.* [16]. Both methods have proved to be more effective than the conventional wavelet-based denoising methods. However, no efforts have been made to adapt PCA-based denoising to SAR images. Since SAR images assume signal-dependent noise, a new denoising model that takes into account this particularity is required.

A different line of research initiated in [18] approaches image denoising as a nonlocal means (NLM) problem, where "nonlocal" pixels whose neighborhoods share similar spatial

Manuscript received June 21, 2012; revised October 15, 2012, June 25, 2013, and December 25, 2013; accepted January 30, 2014. Date of publication March 4, 2014. The work of L. Xu and J. Peng were supported in part by National Natural Science Foundation of China under Grants 41330634, 41374016, and 41304012. *(Corresponding author: J. Li.)*

L. Xu and Y. Shu are with the Department of Geography and Environmental Management, University of Waterloo, Waterloo, ON N2L 3G1, Canada.

J. Li is with the Key Laboratory of Underwater Acoustic Communication and Marine Information Technology (MOE), Xiamen University, China and also with the Department of Geography and Environmental Management University of Waterloo, Waterloo, ON, N2L 3G1, Canada (e-mail: junli@xmu.edu.cn; junli@waterloo.ca).

J. Peng is with the School of Land Science and Techniques, China University of Geosciences, Beijing 100083, China.

Digital Object Identifier 10.1109/TGRS.2014.2304298

structure, rather than "local" pixels that are just geometrically near to each other are used to perform weighted average with the weights measured by the Euclidean distances between the referenced image patch and the other candidate patches. In [19]–[21], the NLM method has been adapted for SAR image denoising by adjusting the similarity measure to the multiplicative nature of speckle noise. In particular, the probabilistic patch-based (PPB) algorithm in [21] proved to achieve the state-of-the-art performance for SAR image denoising. Moreover, the idea of NLM has been extended to combine with the transformed domain denoising approaches, leading to the state-of-the-art image denoising techniques, e.g., the block-matching 3-D filtering (BM3D) [22], LPG-PCA [16], and SAR-BM3D [30] algorithms. All methods take advantage of the enhanced sparsity in transformed domain when denoising is performed on image patches with similar structure. In these methods, block-matching approach was adopted to find, for each patch in the image, a group of similar patches. However, this approach faces the difficulty to define the threshold as to how "similar" to the reference patch is acceptable. It also has high computational cost.

In this paper, we extend this line of study to denoise SAR images by explicitly addressing two issues. First, we build a new denoising model based on PCA technique to account for the multiplicative nature of speckle noise. Based on the ASDN model, we derive an LMMSE approach for solving PCA-based denoising problems. Our approach is the first to build the PCA-based denoising method on the ASDN model for SAR image denoising. Besides SAR images, it is also applicable to other signal-dependent noise. Second, instead of using block-matching approach, we employ a clustering approach. We propose to use the combination of log-transformation, PCA, and K-means methods for finding similar patches. Based on the statistical property of speckle noise, we proved the compatibility between the PCA features and the K-means model. This clustering approach proved to be a competitive alternative to the block-matching approach adopted in [16], [21], and [22].

The rest of this paper is organized as follows. Section II discusses data formation and PCA analysis. Section III derives the LMMSE filtering of speckle noise in PCA domain. Section IV details the clustering-based scheme for SAR image denoising. In Section I, the complete procedure of the proposed strategy that involves a second stage is discussed. In Section VI, experiments are designed to compare the proposed method with other popular denoising techniques. Results obtained using both simulated and real SAR images are presented and discussed. Section VII concludes this study.

II. Data Formation and PCA Analysis

The SAR image as a collection of all of the image patches is represented by a data matrix

$$\mathbf{Y} = [\boldsymbol{y}_1, \boldsymbol{y}_2, \ldots, \boldsymbol{y}_n]^T \tag{1}$$

where n denotes the number of pixels and $\boldsymbol{y}_i (i = 1, 2 \ldots, n)$ is a $p \times 1$ vector, representing the ith patch which is a small square window centered at the ith pixel.

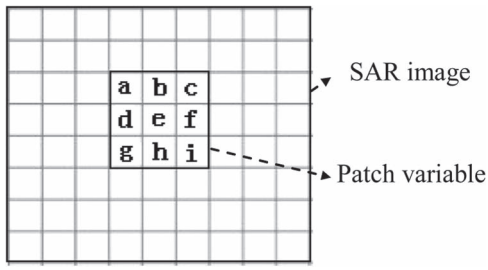

Fig. 1. Illustration of the acquisition of a patch in SAR image.

The PCA can be achieved by performing singular value decomposition (SVD) on the covariance matrix of $\mathbf{Y}$

$$\begin{aligned}\boldsymbol{\Sigma_y} &= \begin{pmatrix} C_{aa} & C_{ab} & \cdots & C_{ai} \\ C_{ba} & C_{bb} & \cdots & C_{bi} \\ \vdots & \vdots & \ddots & \vdots \\ C_{ia} & C_{ib} & \ldots & C_{ii} \end{pmatrix} \\ &= \begin{pmatrix} \boldsymbol{w}_1^T \\ \boldsymbol{w}_2^T \\ \vdots \\ \boldsymbol{w}_p^T \end{pmatrix}^T \begin{pmatrix} \lambda_1 & 0 & \cdots & 0 \\ 0 & \lambda_2 & \cdots & 0 \\ \vdots & \vdots & \ddots & \vdots \\ 0 & 0 & 0 & \lambda_p \end{pmatrix} \begin{pmatrix} \boldsymbol{w}_1^T \\ \boldsymbol{w}_2^T \\ \vdots \\ \boldsymbol{w}_p^T \end{pmatrix}\end{aligned} \tag{2}$$

where element C_{AB} in $\boldsymbol{\Sigma}_{\mathbf{y}}$ represents the covariance between the two pixels at position A and B across the image (see Fig. 1). Therefore, $\boldsymbol{\Sigma_y}$ provides a statistical description of the relationship among pixels in the SAR image. Pixels that do not belong to the same patch are considered uncorrelated. Thus, the size of the patch determines the scale of spatial patterns that can be captured. Generally speaking, a bigger sized patch considers larger range correlations and hence is more capable of capturing larger scale repeated patterns in the SAR image. $\boldsymbol{w}_i (i = 1, \ldots, p)$, $p \times 1$ vectors, denote the sequence of mutually orthogonal PCA bases onto which the projection of patches stack $\mathbf{Y}$ produces the PCs with sequentially largest variances represented by $\lambda_i (i = 1, \ldots, p)$.

In PCA domain, several leading PCs capture most of the scene signal in image patches, while the last few components are mostly due to noise. In this paper, we use PCA for both denoising and feature extraction. In Section III, we develop an LMMSE criterion based on the ASDN model to shrink the PCs. Thus, denoising can be achieved by reconstructing the SAR image using the processed PCs. In Section IV, we use several leading PCs in the logarithmic space identified by the minimum description length (MDL) criterion to feed the K-means algorithm. This not only reduces the dimensionality and decorrelates the spatial variables but also suppresses the noise contained in image patches.

III. SAR Image Denoising in PCA Domain

In [15] and [16], the LMMSE shrinkage was conducted in PCA domain to remove AWGN. For SAR speckle noise, we can certainly adopt the homomorphic approach and apply the same methods in [15] and [16]. However, since the performance of denoising is sensitive to log-transformation that tends to distort the radiometric dynamics of the SAR data, it is more appropriate to perform denoising in original space instead of

logarithmic space. In this section, we derive a new LMMSE shrinkage approach under the ASDN model. We assume that the speckle noise is fully developed; thus, a SAR image pixel can be modeled as

$$y = sx \tag{3}$$

where x, s, and y represent, respectively, the unobserved scene signal, speckle noise, and observed signal. Based on (3), we get the ASDN model as

$$y = x + n \tag{4}$$

where $n = x(s-1)$. Because s has unit mean, thus n is a zero-mean signal-dependent noise. Hence, the patch variable in the SAR image can be described by

$$\boldsymbol{y} = \boldsymbol{x} + \boldsymbol{n} \tag{5}$$

where $\boldsymbol{y} = [y_1, y_2, \ldots, y_p]^T$, $\boldsymbol{x} = [x_1, x_2, \ldots, x_p]^T$, and $\boldsymbol{n} = [n_1, n_2, \ldots, n_p]^T$. Denoting the covariance between y_i and y_j by σ_y^{ij} and the mean of y_i by μ_y^i, we can get

$$\begin{aligned}\sigma_y^{ij} &= E\left[\left(y_i - \mu_y^i\right)\left(y_j - \mu_y^j\right)\right] \\ &= E\left[\left(x_i s_i - \mu_y^i\right)\left(x_j s_j - \mu_y^j\right)\right].\end{aligned} \tag{6}$$

For fully developed speckle noise, x and s are uncorrelated, so we get $E(xs) = E(x)E(s)$. Because $E(s) = 1$, we get $E(y) = E(x)E(s) = E(x)$. Therefore,

$$\begin{aligned}\sigma_y^{ij} &= E(x_i x_j)E(s_i s_j) - \mu_y^j \mu_y^i \\ &= \left[\mu_x^i \mu_x^j + \sigma_x^{ij}\right]\left[1 + \sigma_s^{ij}\right] - \mu_y^j \mu_y^i \\ &= \mu_y^i \mu_y^j + \mu_x^i \mu_x^j \sigma_s^{ij} + \sigma_x^{ij} + \sigma_x^{ij}\sigma_s^{ij} - \mu_y^j \mu_y^i \\ &= \sigma_x^{ij} + \sigma_s^{ij} E(x_i x_j).\end{aligned} \tag{7}$$

We assume that the speckle noise is spatially uncorrelated, i.e., $\sigma_s^{ij} = 0$ for $i \neq j$. Thus, we have

$$\sigma_y^{ij} = \sigma_x^{ij} \text{ (for } i \neq j). \tag{8}$$

In the following analysis, we represent the empirical mean of the patches in $\mathbf{Y}$ by $\bar{\boldsymbol{Y}}$, and we assume that the patch variable $\boldsymbol{y}$ has been centralized. Denoting the covariance of $\boldsymbol{y}$ by $\boldsymbol{\Sigma_y}$, the PCA bases can be obtained by performing SVD on $\boldsymbol{\Sigma_y}$

$$\boldsymbol{\Sigma}_{\mathbf{y}} = \mathbf{W}\boldsymbol{\Lambda}\mathbf{W}^T \tag{9}$$

where the column vectors in $\mathbf{W}$ represent the PCA bases with sequentially largest variances and $\boldsymbol{\Lambda}$ is the diagonal matrix of the variances of PCs, which are the projection of patch variables onto PCA bases

$$\boldsymbol{p} = \mathbf{W}^T\boldsymbol{y} = \mathbf{W}^T\boldsymbol{x} + \mathbf{W}^T\boldsymbol{n} = \boldsymbol{p_x} + \boldsymbol{p_n} \tag{10}$$

where $\boldsymbol{p_x} = \mathbf{W}^T\boldsymbol{x}$ and $\boldsymbol{p_n} = \mathbf{W}^T\boldsymbol{n}$ stand, respectively, for the signal and noise parts in the projection. If $\boldsymbol{p_x}$ is known, denoising can be achieved by performing inverse PCA transformation using $\boldsymbol{p_x}$. In this paper, $\boldsymbol{p_x}$ is estimated by the LMMSE criterion

$$\begin{aligned}\widehat{\boldsymbol{p_x}} &= E(\boldsymbol{p_x}) + \mathrm{Cov}(\boldsymbol{p_x}, \boldsymbol{p})\boldsymbol{\Sigma}_{\mathbf{p}}^{-1}\left(\boldsymbol{p} - E(\boldsymbol{p})\right) \\ &= 0 + \boldsymbol{\Sigma}_{\mathbf{p_x}}\boldsymbol{\Sigma}_{\mathbf{p}}^{-1}(\boldsymbol{p} - 0) = \boldsymbol{\Sigma}_{\mathbf{p_x}}\boldsymbol{\Lambda}^{-1}\boldsymbol{p}.\end{aligned} \tag{11}$$

The ijth element of $\boldsymbol{\Sigma}_{\boldsymbol{p_x}}$ can be estimated through the following equation:

$$\begin{aligned}\sigma_{p_x}^{ij} &= E\left(p_x(i)p_x(j)\right) - \mu_{p_x}^i \mu_{p_x}^j \\ &= E\left\{\left[\boldsymbol{W}^T(i,:)\boldsymbol{x}\right]\left[\boldsymbol{W}^T(j,:)\boldsymbol{x}\right]\right\} - \boldsymbol{W}^T(i,:)\boldsymbol{\mu_x}\boldsymbol{W}^T(j,:)\boldsymbol{\mu_x} \\ &= E\left\{\sum_k W(k,i)x_k \sum_t W(t,j)x_t\right\} \\ &\quad - \sum_k W(k,i)\mu_x^k \sum_t W(t,j)\mu_x^t \\ &= E\left\{\sum_k \sum_t W(k,i)W(t,j)x_k x_t\right\} \\ &\quad - \sum_k \sum_t W(k,i)W(t,j)\mu_x^k \mu_x^t \\ &= \sum_k \sum_t W(k,i)W(t,j)\left[E(x_k x_t) - \mu_x^k \mu_x^t\right] \\ &= \sum_k \sum_t W(k,i)W(t,j)\sigma_x^{kt} \\ &= \Sigma_k W(k,i)W(k,j)\sigma_x^k + \Sigma_k \Sigma_{t,t\neq k} W(k,i)W(t,j)\sigma_x^{kt}.\end{aligned} \tag{12}$$

Denote $u_j = s_j - 1$. Because x_j and u_j are uncorrelated for fully developed speckle noise, we can get

$$\begin{aligned}E\left(y_j^2\right) &= E\left[(x_j + x_j u_j)^2\right] \\ &= E\left(x_j^2\right) + E\left(x_j^2 u_j^2\right) \\ &= E\left(x_j^2\right)(1 + \sigma_u).\end{aligned} \tag{13}$$

From (13) and (7), we get $\sigma_x^k = \sigma_y^k - (\sigma_u/\sigma_u + 1)E(y_k^2)$, so

$$\begin{aligned}\sigma_{p_x}^{ij} = \Sigma_k W(k,i)W(k,j)&\left[\sigma_y^k - \frac{\sigma_u}{\sigma_u + 1}E\left(y_k^2\right)\right] \\ &+ \Sigma_k \Sigma_{t,t\neq k} W(k,i)W(t,j)\sigma_x^{kt}.\end{aligned} \tag{14}$$

From (8), we get $\sigma_x^{kt} = \sigma_y^{kt}$ for $t \neq k$, so

$$\begin{aligned}\sigma_{p_x}^{ij} = \Sigma_k W(k,i)W(k,j)&\left[\sigma_y^k - \frac{\sigma_u}{\sigma_u + 1}E\left(y_k^2\right)\right] \\ &+ \Sigma_k \Sigma_{t,t\neq k} W(k,i)W(t,j)\sigma_y^{kt}.\end{aligned} \tag{15}$$

In (15), σ_u can be calculated from the theoretical distribution of speckle noise, e.g., for gamma distribution $\sigma_u = 1/L$[12], where L stands for the ENL. $W(i,j)$ is the ijth element of $\mathbf{W}$ in (9). $E(y_k^2)$ and σ_y^{kt} are estimated by the respective empirical values: $E(y_k^2) = \Sigma_y(k,k) + \bar{Y}^2(k)$, and $\sigma_y^{kt} = \Sigma_y(k,t)$, where $\Sigma_y(i,j)$ stands for the ijth element of $\boldsymbol{\Sigma}_{\mathbf{y}}$ and $\bar{Y}(i)$ stands for the ith element of $\bar{\boldsymbol{Y}}$.

Given $\widehat{\boldsymbol{P_x}}$ in (11), the noise-free image patch can be obtained by performing inverse PCA transformation

$$\widehat{\boldsymbol{y}} = \overline{\boldsymbol{Y}} + \mathbf{W}\widehat{\boldsymbol{p_x}}. \tag{16}$$

The denoised patches will finally be used to construct the noise-free SAR image.

IV. Clustering Scheme

The effectiveness of denoising in PCA domain depends highly on whether the PCs can sparsely represent the scene signal. Moreover, the sparsity can be achieved by performing analysis on patches with similar spatial structure. There are two approaches for finding similar patches, namely, block-matching and clustering. Block-matching is a supervised approach, which finds, for each pixel on the image, a group of patches that are "similar" to the reference patch. This approach has high computational cost. Since it is hard to define the "threshold" as to how "similar" to the reference patch is acceptable, the researchers always turn to guarantee a minimum number of similar patches. However, it may render some of the selected patches less relevant to the referenced patch. As opposed to the block-matching approach adopted in BM3D and NLM, the clustering approach involved in the proposed approach finds similar patches in an unsupervised manner by adaptively partitioning the image into disjoint areas. It requires less computation. Moreover, since the "threshold" in the clustering approach is adaptively determined by comparing the proximities of the candidate patch to different cluster centers, rather than being predefined, the clustering approach is supposed to be more capable of finding relevant patches than the block-matching approach.

In this paper, we adopt the K-means algorithm [27] proposed by Lloyd considering its simplicity and speed. Moreover, we use the Euclidean distance to measure similarity in feature space. Performing K-means clustering on image patches also faces problems, such as high dimensionality, high correlation among features, and intense iterations due to poor initial parameter values. In this paper, we adopt log-transformation and PCA to extract compact features to feed the K-means algorithm.

This section is organized as follows: we start with the illustration of feature extraction techniques, we then prove the compatibility of the extracted features and K-means algorithm, and lastly, we discuss parameter tuning and efficient realizations of the clustering algorithm.

A. Feature Extraction

Before extracting features for clustering, we apply log-transformation on the original SAR image as a preprocessing step. It has been common practice to aid clustering by preprocessing heavy tail distributed variables using log-transformation [23], [24]. In particular, Liu [23] indicated that log-transformation significantly improved the clustering result, and Paxson [24] demonstrated a 10% increase in clustering accuracy after applying the log-transformation. The speckle noise in the SAR image follows gamma distribution that is long tailed. Moreover, the speckle noise is signal dependent, which means that it has a bigger variance on brighter image areas. This unstable nature would produce large between-cluster overlapping. Therefore, the log-transformation is used here to deskew the data set and to stabilize the variance. The log-transformed data tend to be symmetrically distributed with constant variance; thus, they are more desirable for statistical methods, such as PCA and K-means algorithms.

Although clustering can be performed directly on image patches, it always suffers from high dimensionality, e.g., a 5×5 patch produces 25 variables, and the intense speckle noise contained in the patch. In order to solve these problems, we adopt PCA as a feature extraction technique. Only K leading PCs that are mostly due to the signal are used as features for clustering. The accurate estimation of K is important in the sense that the underestimation would lose useful information, but overestimation would introduce noise and unnecessary computation cost. One popular approach determines K by setting a threshold to the percentage of variation explained by signal components. This approach is simple but rather subjective. In this paper, we estimate K by the MDL criterion which was proposed by Rissanen in [25] and which has been used to determine the number of signals in [26]. The $p \times 1$ dimensional image patch variable $\vec{\boldsymbol{y}}$ subject to log-transformation can be represented by the following equation:

$$\vec{\boldsymbol{y}} = \sum_{i=1}^{K} \overrightarrow{\boldsymbol{W}}(:,i)\vec{p}_i + \vec{\boldsymbol{n}} \tag{17}$$

where $\overrightarrow{\mathbf{W}}$ is the eigenvector matrix, whose ith column $\overrightarrow{\boldsymbol{W}}(:,i)$ denotes the ith PCA bases, and $\vec{\boldsymbol{n}}$ denotes the log-transformed speckle noise that roughly satisfies Gaussian distribution with zero mean and diagonal covariance matrix $\mathbf{I}_{\mathrm{p}}\sigma_{\vec{n}}$. We assume that the scene signal $\vec{\boldsymbol{x}}$ can be reconstructed by the first K PCs

$$\vec{\boldsymbol{x}} = \sum_{i=1}^{K} \overrightarrow{\boldsymbol{W}}(:,i)\,\vec{p}_i \tag{18}$$

where $\vec{p}_i = \vec{\boldsymbol{x}}^T\,\overrightarrow{\boldsymbol{W}}(:,i)$ stands for the ith PC. We can see that (17) is the same with (1) in [26], where Wax and Kailath estimated the number of signals by

$$K_{\mathrm{MDL}} = \arg\min_{k}(p-k)\log\frac{\sum_{k+1}^{p}\lambda_j}{p-k} - \log\prod_{k+1}^{p}\lambda_j + \frac{k(2p-k)}{2n}\log n \tag{19}$$

where λ_j stands for the jth biggest eigenvalue of $\boldsymbol{\Sigma}_{\vec{\boldsymbol{y}}}$ and n denotes the number of observations.K_{MDL} can be easily determined by comparing all of the $p-1$ solutions.

B. Compatibility of PCA Features and K-Means Algorithm

K-means algorithm that relies on Euclidean distance implicitly assumes that the noise of input features satisfies independent and identically Gaussian distribution. In the following, we prove that PCA features described previously satisfy this assumption. We reformulated (17) as

$$\vec{\boldsymbol{y}} = \vec{\boldsymbol{x}} + \vec{\boldsymbol{n}}. \tag{20}$$

Since $\vec{\boldsymbol{x}}$ and $\vec{\boldsymbol{n}}$ are independent for fully developed speckle noise, we can get

$$\boldsymbol{\Sigma}_{\vec{\boldsymbol{y}}} = \boldsymbol{\Sigma}_{\vec{\boldsymbol{x}}} + \sigma_{\vec{n}}\mathbf{I}_p \tag{21}$$

where $\mathbf{\Sigma}_{\vec{y}}$ and $\mathbf{\Sigma}_{\vec{x}}$ denote, respectively, the covariance matrices of $\vec{y}$ and $\vec{x}$. The PCA analysis can be achieved by performing SVD on $\mathbf{\Sigma}_{\vec{x}}$:

$$\mathbf{\Sigma}_{\vec{x}} = \overrightarrow{\mathbf{W}}\,\overrightarrow{\mathbf{S}}\,\overrightarrow{\mathbf{W}}^{T} \tag{22}$$

where the column vectors in $\overrightarrow{\mathbf{W}}$ represent the PCA bases and $\overrightarrow{\mathbf{S}} = \mathrm{diag}(s_1, \ldots, s_p)$ is an eigenvalue matrix.

Then, we have

$$\begin{aligned}\mathbf{\Sigma}_{\vec{y}} &= \overrightarrow{\mathbf{W}}\,\overrightarrow{\mathbf{S}}\,\overrightarrow{\mathbf{W}}^{\boldsymbol{T}} + \sigma_{\vec{n}}\overrightarrow{\mathbf{W}}\overrightarrow{\mathbf{W}}^{\boldsymbol{T}} \\ &= \overrightarrow{\mathbf{W}}\begin{bmatrix} s_1 + \sigma_{\vec{n}} & \cdots & 0 \\ \vdots & \ddots & \vdots \\ 0 & \cdots & s_p + \sigma_{\vec{n}} \end{bmatrix}\overrightarrow{\mathbf{W}}^{\boldsymbol{T}}. \end{aligned} \tag{23}$$

Therefore, we can see that $\mathbf{\Sigma}_{\vec{x}}$ and $\mathbf{\Sigma}_{\vec{y}}$ share the same PCA bases. As in (10), the PCA features can be obtained by projecting the image patch onto PCA bases

$$\vec{p} = \overrightarrow{\mathbf{W}}^{\boldsymbol{T}}\vec{y} = \overrightarrow{\mathbf{W}}^{\boldsymbol{T}}\vec{x} + \overrightarrow{\mathbf{W}}^{\boldsymbol{T}}\vec{n} = \vec{p}_{\,x} + \vec{p}_{\,n} \tag{24}$$

where $\vec{p}_{\boldsymbol{x}} = \overrightarrow{\mathbf{W}}^{\boldsymbol{T}}\vec{x}$ and $\vec{p}_{\boldsymbol{n}} = \overrightarrow{\mathbf{W}}^{\boldsymbol{T}}\vec{n}$ stand, respectively, for the signal and noise parts in the PCA feature. Denote the variance matrix of $\vec{p}$ by $\mathbf{\Sigma}_{\vec{p}}$

$$\mathbf{\Sigma}_{\vec{\mathbf{p}}} = \mathbf{\Sigma}_{\vec{\mathbf{p}}_{\mathbf{x}}} + \mathbf{\Sigma}_{\vec{\mathbf{p}}_{\mathbf{n}}} = \begin{bmatrix} s_1 & \cdots & 0 \\ \vdots & \ddots & \vdots \\ 0 & \cdots & s_p \end{bmatrix} + \begin{bmatrix} \sigma_{\vec{n}} & \cdots & 0 \\ \vdots & \ddots & \vdots \\ 0 & \cdots & \sigma_{\vec{n}} \end{bmatrix}. \tag{25}$$

Since $\mathbf{\Sigma}_{\vec{\mathbf{p}}_{\mathbf{n}}} = \sigma_{\vec{n}}\mathbf{I}_p$, the assumption of K-means algorithm on noise distribution can be well satisfied. Although this property could not guarantee the convergence of K-means algorithm to global minimum, it provides theoretical assurance that K-means performance can be optimized.

C. Parameter Tuning and Efficient Realization

1) Number of Clusters: The number of clusters T in the image depends on the definition of what constitutes a cluster. This issue is mostly application oriented, e.g., for background subtraction, background and foreground should be represented as two clusters, but in content-based image analysis, the number of cluster is mainly determined by the number of objects in the image. Here, we have no high-level requirements on the notion of cluster but only a loose constraint that a cluster is a collection of image patches with similar spatial structures. Thus, the number of clusters cannot be and does not need to be estimated very accurately. A loose cluster can be split into several compact ones, which does not have too much influence on the denoising results. Nevertheless, the rough estimation of the number of patterns that exist in the image is still important because over underestimation would reduce the sparsity in PCA domain, and the opposite would increase computation burden and also preserve unnecessary artifact. Therefore, the number of clusters can be better determined based on the complexity of the scene. A more complex image should be assigned more clusters to fully capture image details. Since PCA detects statistically uncorrelated sources, a more complex image scene tends to have a larger number of signal PCs. Therefore, we use the number of signal PCs K_{MDL} in Section IV-A as the estimate of the number of clusters. Moreover, to prevent oversegmentation, we set an upper limit on T. In this paper, we require

$$T = \max(K_{\mathrm{MDL}}, 15). \tag{26}$$

2) Size of Cluster: The number of patches in each cluster should be big enough for efficient estimation of the covariance matrix $\mathbf{\Sigma}_{\boldsymbol{y}}$. In this paper, we constrain that each cluster should have at least 50 members. A cluster smaller than this value will be deleted, and its members will be dispersed into the other clusters based on the proximity in Euclidean space.

3) Initial Cluster Centers: K-means clustering is very sensitive to initial parameter values. Poor assignment of initial parameters may cause longer time to converge. Because the PCs provide a contiguous membership indicator for K-means clustering [28], we estimate the labels of image pixels by sorting the values of the first PC and then splitting them evenly into T groups. Given the initial labels, we estimate the centroids for each group.

4) Deal With Large Image: SAR images always have a big size. Clustering on them directly tends to ignore weak patterns that involve a small number of pixels. Hence, some image details would be erased during the denoising stage. Therefore, in this study, a large image is divided into several subimages which are denoised separately. The final noise-free image is reconstructed by all of the denoised subimages. There is no universal standard for the size of the subimage. It should be adjusted according to the complexity of the image scene. A small size should be preferred for an image with a complex scene. For the SAR image, a size of 64 $\times$ 64 pixels can achieve a good result based on our experiments. To avoid the boundary artifacts between neighboring subimages, we design the neighboring subimages to be slightly overlapping. Based on our experiment, an overlapping of 5 pixels would produce smooth boundaries.

5) Size of Patch: As discussed in Section III, a patch with big size can capture large-scale patterns but would also increase the computation cost. For SAR images that are without strong texture patterns, the size of 3 $\times$ 3 pixel is sufficient according to our experiments. However, a larger patch size, such as 5 $\times$ 5, is required for heavily textured images (Fig. 1).

V. Complete Procedure of the Proposed Approach

The complete procedure involves two stages (Fig. 2): the first stage produces a denoised image which is referenced as a clean image in the second stage to feed the clustering algorithm and to aid the LMMSE shrinkage. The detailed procedure is given in the following.

Stage 1: The original SAR image is split into N subimages which are $M \times M$ sized $(M = 64)$. For each subimage, we repeat the steps of clustering and denoising until all subimages have been processed. Finally, we aggregate the denoised patches to produce the denoised SAR image.

1) *Clustering*: This step intends to identify image pixels whose neighborhoods have a similar spatial structure. The ith subimage is first log-transformed. Then, we extract all

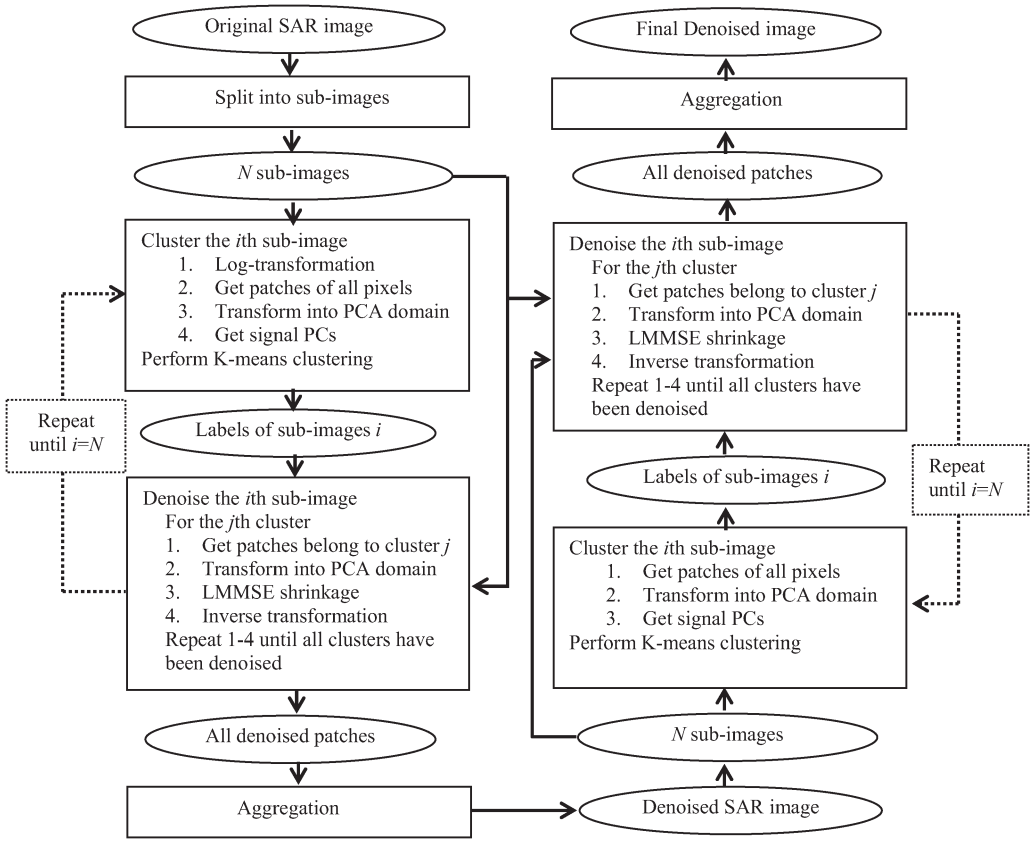

Fig. 2. Flowchart of the proposed algorithm (left part: stage 1; right part: stage 2).

of the $S \times S$ sized patches $(S = 5)$ to form a data matrix which is then transformed into the PCA domain. The first K_{MDL} PCs are used to feed the K-means algorithm, where K_{MDL} is given in Section IV-A. The number of cluster is determined by (26). Other parameters, i.e., the size of the cluster and the initial cluster centers, are given in Section IV-C. The products of this step are the labels of all pixels in the ith subimage.

2) *Denoising*: Given the labels, this step aims to denoise the ith subimage. Image patches in each cluster are denoised separately. Note that the image patches are extracted from the original SAR image. For each cluster, patches of pixels that belong to this cluster are extracted to form a data matrix. We calculate the empirical mean $\bar{\boldsymbol{Y}}$ and variance matrix $\boldsymbol{\Sigma_y}$. Then, the patches are denoised by the following operations: obtaining PCA bases (9), projecting onto PCA bases (10), shrinking PCs in PCA domain (11) and (15), and transforming back into patch domain (16). This step does not stop until all of the clusters in the ith subimage have been denoised. The final product of this step is a collection of denoised patches in the ith subimage.

3) *Aggregation*: In this step, the denoised patches are used to construct the noise-free image. Because the patches are overlapping, each pixel in the image has many denoised values. The final value is estimated as their average. The final product of this step is a denoised image.

Stage 2: This stage goes through the same operations as stage 1, except that we use the denoised image in stage 1 to feed the clustering step and to aid the LMMSE shrinkage in the denoising step.

1) *Clustering*: Instead of the original SAR image, the denoised image produced in stage 1 is used for clustering to get the labels. Moreover, the log-transformation is avoided. Other operations are the same with stage 1.

2) *Denoising*: The denoising procedures on this stage are the same with stage 1, except that we use the denoised image in stage 1 to estimate $\boldsymbol{\Sigma}_{\mathbf{p_x}}$ in (11). Given labels, we extract two sets of patches for each cluster. One set is from the original SAR image. This set is to be denoised. Another set is from the denoised image produced by stage 1. This set is treated as a collection of signal patches. Hence, the covariance matrix of signal patches $\widehat{\boldsymbol{\Sigma}}_{\mathbf{x}}$ can be estimated as the sample covariance matrix. The shrinkage of the first set of patches in PCA domain requires the estimation of $\boldsymbol{\Sigma}_{\mathbf{p_x}}$. Here, instead of using (15), we use

$$\boldsymbol{\Sigma}_{\mathbf{p_x}} = \mathbf{W}^{\mathbf{T}} \widehat{\boldsymbol{\Sigma}}_{\mathbf{x}} \mathbf{W}. \tag{27}$$

3) *Aggregation*: The denoised patches are used to estimate the final noise-free image. The aggregation procedures are the same with stage 1.

Stage 2 is basically a repetition of stage 1, except that we used the denoised image in stage 1 to perform clustering and to estimate $\boldsymbol{\Sigma}_{\mathbf{p_x}}$ in (11). These modifications are motivated by the fact that the first stage can significantly suppress SAR speckle noise and achieve a cleaner image. Hence, using the denoised image, instead of the noisy image, can achieve more accurate

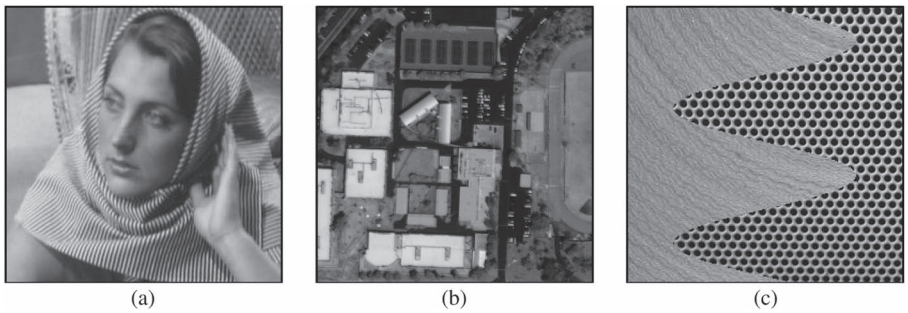

Fig. 3. Clean images used in this paper. (a) Barbara. (b) Optical satellite image (IKONOS). (c) Synthesized texture image. All images are 256 × 256 pixels big.

clustering results. Moreover, treating the denoised image as a clean image to estimate $\mathbf{\Sigma}_{\mathbf{p_x}}$ is more efficient than performing shrinking on the noisy image. A second stage in the BM3D algorithm [21] was motivated by similar considerations.

VI. Results and Discussion

In this paper, both simulated and real SAR images are used to test the proposed SAR denoising method. In order to achieve a quantitative evaluation, clean images are degraded by adding multiplicative noise. Thus, we can treat the clean image as the true values and use numerical measures to evaluate the performance. Although the true values of real SAR images are unknown, we can achieve qualitative assessments based on visual interpretation. In this experiment, three other methods (i.e., PPB [21], LPG-PCA [16], and SAR-BM3D algorithms [30]) are selected to compare with the proposed method. The selection of these methods is based on the considerations of both the availability of the codes and their relevance to our work. The LPG-PCA represents the state-of-the-art denoising techniques for images with additive noise, while PPB and SAR-BM3D are the state-of-the-art methods for the SAR image. Because LPG-PCA was designed to deal with additive noise, to adapt it to the SAR image, we transform the speckle noise into additive noise by logarithmic operation before performing it on noisy SAR images. The biased means caused by log-transformation are also corrected. In all experiments, without explicit indication, the parameters of the aforementioned algorithms are set as suggested in the referenced papers, and our method is implemented by setting the patch size to 5 × 5 pixels and the subimages to 64 × 64 pixels, with 5 pixels overlapping with their neighbors. All of the other parameters in our method are determined by the methods in Section IV-C.

A. Test With Simulated Images

A variety of image sources are considered in this experiment, including the benchmark test image, i.e., Barbara [Fig. 3(a)] in the image denoising literature, and the high-resolution optical satellite (i.e., IKONOS) image whose scene structure is similar to a real SAR image [Fig. 3(b)]. An ideal SAR denoising method is required to be capable of removing speckle effectively while in the meantime preserving image details (e.g., texture, edge, and line target) that constitute the desired features for further analysis. Therefore, in order to fully examine the abilities of detail preservation, an image comprising two texture parts with a smooth boundary is designed to be used in this experiment. As shown in Fig. 3(c), the left part of the image is weakly textured with a wave-like appearance, while the right part is with a strong mesh texture. Thus, the performance of denoising methods on an image with changing scene complexities can be investigated. Simulated SAR images are obtained by multiplying speckle noise with these clean images. In this experiment, we use speckle noise in amplitude format which satisfies a squared-root gamma distribution [12]. All images are degraded with four different levels of speckle noise, i.e., the ENL (denoted by L) is equal to 1, 2, 4, and 16, respectively. To avoid randomness, 20 noisy images for each clean image are produced by multiplying different noise realizations. All noisy images are processed, and the numerical evaluation is based on the average of the results.

In this paper, two statistics (i.e., signal-to-mean-square-error ratio (S/MSE) and β) are used to evaluate these denoising methods. S/MSE corresponding to SNR in case of additive noise is a very effective measure of noise suppression in multiplicative case [6]. On the other hand, to measure image detail preservation, we employ β originally defined in [29]. β should be equal to unity for an ideal detail preservation.

The zooms of denoised images by different methods when $L = 1$ are shown in Figs. 4–6, and the values of the two statistics for $L = 1, 2, 4$, and 16 are summarized in Table I, in which the best value in each unit is bold. Overall, it shows in Table I that the proposed method outperformed the other referenced algorithms in terms of both measures. This demonstrates that our method is good both at speckle noise suppression and image detail preservation. The row "prop.stage1" in Table I was achieved by the first stage of our method. Comparing with row "prop.," we can see that the second stage involved in our method can significantly improve the results. The row "prop.global" in Table I was achieved by performing PCA denoising on the subimages without the clustering step. The observation that values in "prop.global" are lower than values in "prop." justifies the clustering approach in the proposed method.

Both LPG-PCA and the proposed method denoise SAR images in PCA domain. However, LPG-PCA works on the AWGN obtained by performing log-transformation on the SAR image, while the proposed method takes into account the multiplicative nature of speckle noise by building the denoising approach on the ASDN model. The observation that the proposed method greatly outperformed LPG-PCA on most noise levels justifies the proposed denoising model for ASDN. We also observed that the performance of LPG-PCA is very sensitive to noise

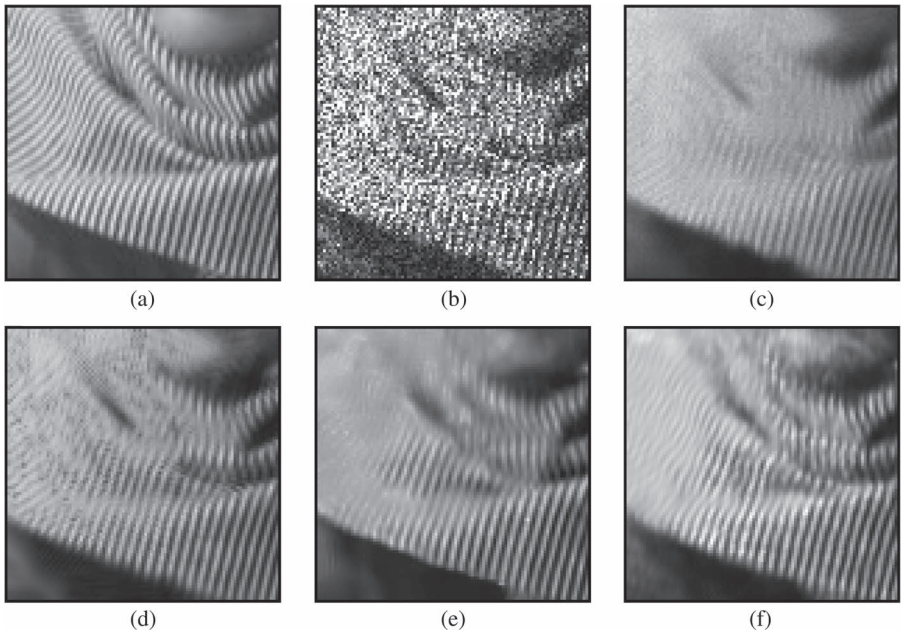

Fig. 4. Zoom of Barbara image degraded by single-look speckle noise. (a) Clean image. (b) Noisy image. (c) PPB. (d) LPG-PCA. (e) SAR- BM3D. (f) Proposed method.

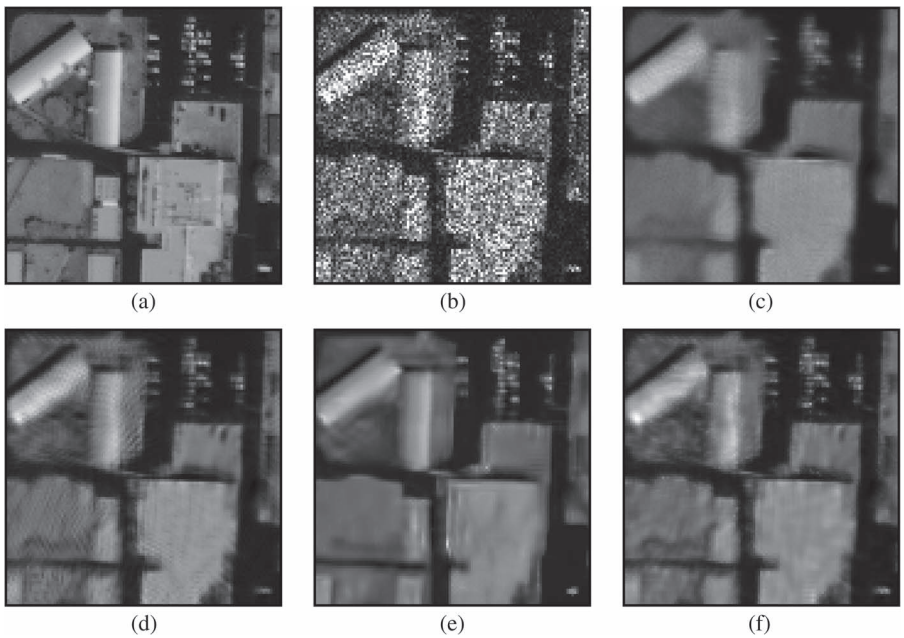

Fig. 5. Zoom of IKONOS image degraded by single-look speckle noise. (a) Clean image. (b) Noisy image. (c) PPB. (d) LPG-PCA. (e) SAR-BM3D. (f) Proposed method.

level variation in logarithmic space. As we can see in Table I, when $L = 1$, LPG-PCA achieved lower statistics than the proposed method. However, with the increase of L, LPG-PCA tends to achieve comparable results with our method in terms of β. LPG-PCA even achieved higher β on image Barbara when $L = 4$ and 16. This is reasonable because LPG-PCA was designed for AWGN. When L is big, the speckle noise subject to logarithmic operation is very close to the Gaussian white noise. Therefore, the method can achieve good results. However, when L is small, speckle noise begins to deviate from Gaussian distribution, and its mean value is no more zero. This discrepancy between the empirical data and the model assumption may reduce the efficiency of LPG-PCA. As we can see, the images in Figs. 4–6 denoised by LPG-PCA show many small artifacts, while images by the proposed method have little artifacts but plenty of image details.

It is noticed that our method was especially better at denoising the synthesized texture image [Fig. 3(c)]. In Fig. 6, the image produced by the proposed method is the most similar to the clean image. The images denoised by PPB and SAR-BM3D are blurred, and the holes in the boundary area are erased. The image produced by LPG-PCA has clear textural

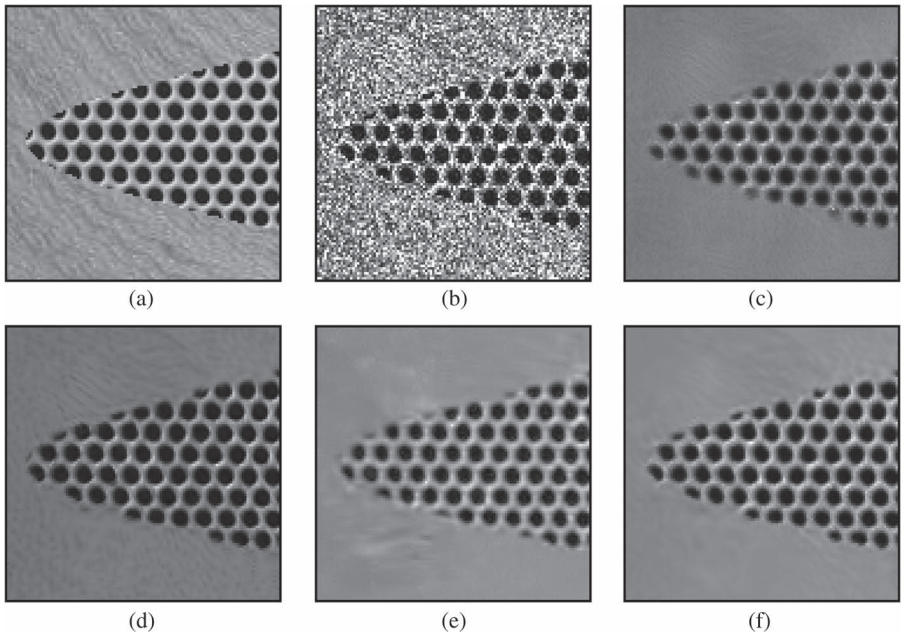

Fig. 6. Zoom of synthesized texture image degraded by single-look speckle noise. (a) Clean image. (b) Noisy image. (c) PPB. (d) LPG-PCA. (e) SAR-BM3D. (f) Proposed method.

TABLE I
RESULTS (S/MSE AND β) ON THREE IMAGES WITH DIFFERENT NOISE LEVELS

		IKONOS				Barbara				Syntexture			
		L=1	L=2	L=4	L=16	L=1	L=2	L=4	L=16	L=1	L=2	L=4	L=16
S/MSE	noisy	6.68	9.35	12.19	18.10	6.69	9.35	12.18	18.11	6.69	9.35	12.18	18.09
	PPB	14.99	16.56	17.97	21.26	16.27	17.08	18.76	19.20	11.41	11.10	11.95	17.76
	LPG-PCA	16.70	18.06	19.43	21.15	16.84	17.11	18.49	19.41	10.73	12.45	14.74	19.99
	SAR-BM3D	14.85	15.04	18.04	21.97	16.93	17.19	17.31	19.58	15.89	17.29	16.55	18.60
	Prop.	**17.17**	**18.10**	**19.70**	22.24	**17.29**	**18.27**	**18.75**	**19.80**	**18.95**	**20.30**	**21.28**	**23.99**
	Prop.stage1	13.89	15.90	18.67	**22.87**	14.83	16.64	17.38	19.46	13.31	15.73	17.59	21.75
	Prop.global	12.25	14.04	15.63	20.05	12.98	14.67	15.71	18.39	10.65	13.06	14.65	18.71
β	noisy	0.183	0.246	0.333	0.572	0.167	0.223	0.304	0.534	0.252	0.335	0.441	0.695
	PPB	0.323	0.470	0.567	0.696	0.519	0.663	0.765	0.873	0.599	0.640	0.697	0.818
	LPG-PCA	0.364	0.527	0.658	0.796	0.616	0.738	**0.852**	**0.917**	0.730	0.791	0.838	0.893
	SAR-BM3D	0.484	0.576	0.658	0.804	0.708	0.771	0.835	0.897	0.663	0.729	0.783	0.783
	Prop.	**0.495**	**0.598**	**0.685**	**0.829**	**0.719**	**0.788**	0.845	0.913	**0.792**	**0.835**	**0.868**	**0.920**
	Prop.stage1	0.376	0.498	0.616	0.804	0.562	0.668	0.760	0.883	0.655	0.751	0.815	0.899
	Prop.global	0.321	0.401	0.491	0.687	0.472	0.576	0.675	0.826	0.522	0.596	0.671	0.812

patterns but assumes many artifacts. The statistics in Table I indicate consistent results. The proposed method achieved high values in both measures, indicating good performance on both noise removal and detail preservation. In contrast, LPG-PCA achieved small S/MSE values, while PPB and SAR-BM3D achieved small β values. The clustering approach involved in the proposed method may have contributed to the superiority of the proposed method in dealing with textual images. In a textured image, the increased scene complexity renders it difficult to find similar patches. Given the difficulty, the clustering approach might find more relevant patches than the block-matching approach, leading to better preservation of texture patterns. On a less-textured image, i.e., IKONOS, the proposed approach also achieved higher β values and preserved more image details than the other methods. The observation that LPG-PCA and the proposed method outperformed SAR-BM3D in terms of detail preservation in highly textured image (i.e., Fig. 6) may suggest that the PCA-based denoising approach is more efficient at dealing textural structures.

A good denoising method should be capable of removing speckle noise without sacrificing image details. PPB tended to erase image details too much. In Figs. 4–6, we see that the denoised images by PPB have very smooth appearances but also blurred boundaries and reduced detail information. On the IKONOS image, LPG-PCA achieved higher S/MSE but lower β values than SAR-BM3D, while on the Syntexture image, LPG-PCA achieved lower S/MSE but higher β values. Our method achieved very high S/MSE and β values on most images.

The SAR-BM3D and PPB algorithms were implemented using the C language, while the other algorithms were implemented under the MATLAB platform. All of the computations were conducted on a personal computer with a Pentium 2.30-GHZ Quad-Core processor. On average, it took

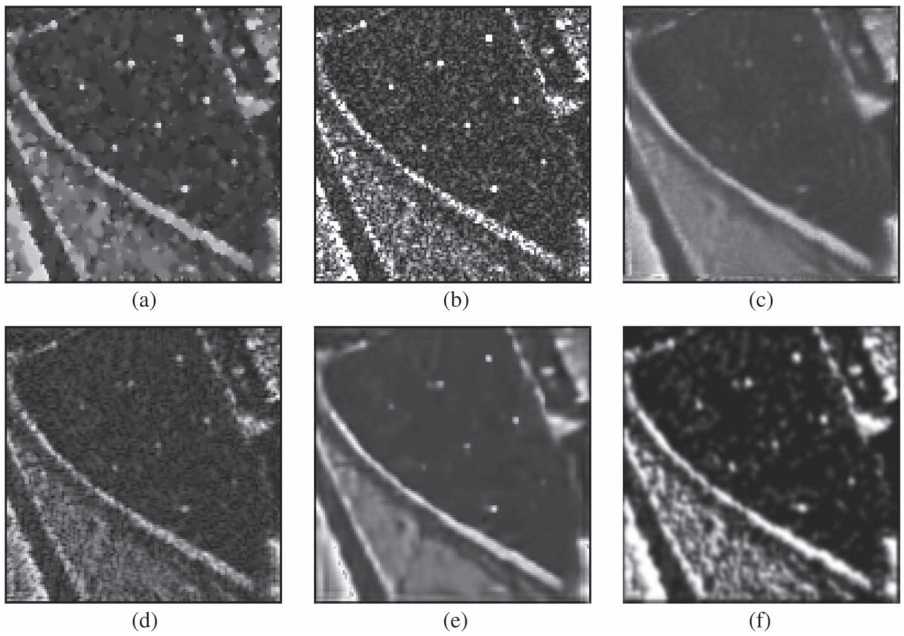

Fig. 7. Zoom of TerraSAR-X SSC image (112 × 95 pixels) of the parking lot located at the NE of the Macdonald-Cartier Freeway/Allen Road interchange, Toronto, ON, Canada, with $L = 1$. (a) SRAD. (b) Original image. (c) PPB. (d) LPG-PCA. (e) SAR-BM3D. (f) Proposed method.

36.8, 53.1, 34.7, and 23.5 s, respectively, for PPB, LPG-PCA, SAR-BM3D, and the proposed method to process a 256 × 256 pixel simulated image. It is fair to compare the time efficiency of the proposed algorithm and LPG-PCA because both methods are PCA-based and implemented in MATLAB language. The observation that the proposed algorithm consumes less than half of the time of LPG-PCA demonstrates the efficiency of the clustering algorithm than the block-matching approach. This conclusion is also supported by the shorter processing time of our algorithm than PPB and SAR-BM3D, especially considering the fact that C language is more efficient than MATLAB.

B. Test With Real SAR Images

The real SAR images used for testing different denoising methods are two TerraSAR-X sample imageries provided on the Astrium GeoInformation Services website. Both images are located at Toronto, ON, Canada, taken in December 2007 under the spotlight mode with 1-m spatial resolution and incidence angle of 48.8°. However, one is the single-look slant range complex (SSC) image, while the other one is the spatially enhanced (SE) multilook ground-range detected (MGD) with $L = 2$. From the SSC image, we obtain two smaller images, and from the MGD image, we obtain one. The three images that comprise parking lots, roads, and buildings are supposed to capture the major types of urban targets.

In this experiment, in addition to the denoising algorithms in the simulated study, we also tested the SRAD method in [4]. We adopted the default patch size parameters for the referenced methods but a smaller size of 3 × 3 for the proposed method because they experimentally allowed the respective best tradeoffs between noise removal and detail preservation. The zooms of these images denoised by different techniques are shown in Figs. 7–9. The results are basically consistent with the simulated study. The proposed method not only greatly suppressed speckle noise, e.g., all three denoised images are very smooth but also preserve image details very well, e.g., the eight bright spots in Fig. 7 were kept very well, and the roads in Fig. 8 were delineated very clearly. The SAR-BM3D also achieved good balance between noise removal and detail preservation. The PPB method achieved very clean images, but some image details were also smoothed out. The LPG-PCA, because it was not specifically designed for SAR speckle noise, produced many dark artifacts in Figs. 7 and 8 where noise level is high but achieved smoother results in Fig. 9 where less noise exists. Generally speaking, SRAD preserved point targets very well but also produced undesirable artifacts.

VII. Conclusion

In this paper, we have presented a SAR image denoising scheme based on clustering the noisy image into disjoint local regions and denoising each region by LMMSE filtering in PCA domain. In the clustering step, in order to reduce dimensionality and resist the influence of noise, we have identified several leading PCs in logarithmic domain by MDL criterion to feed the K-means algorithm. This clustering approach can be treated as the unsupervised counterpart of the commonly adopted block-matching approach. It requires less computation. Moreover, it is capable of adaptively identifying "similar" patches by considering the closeness to different cluster centers. In the denoising stage, in order to avoid the limitations of the homomorphic approach, we have built our denoising scheme on ASDN and derived a PCA-based LMMSE denoising model for multiplicative noise. Our approach is the first to build the PCA-based denoising method on the ASDN model for SAR image denoising. Besides SAR images, it is also applicable to other signal-dependent noise. The denoised patches of all clusters were finally used to reconstruct the noise-free image.

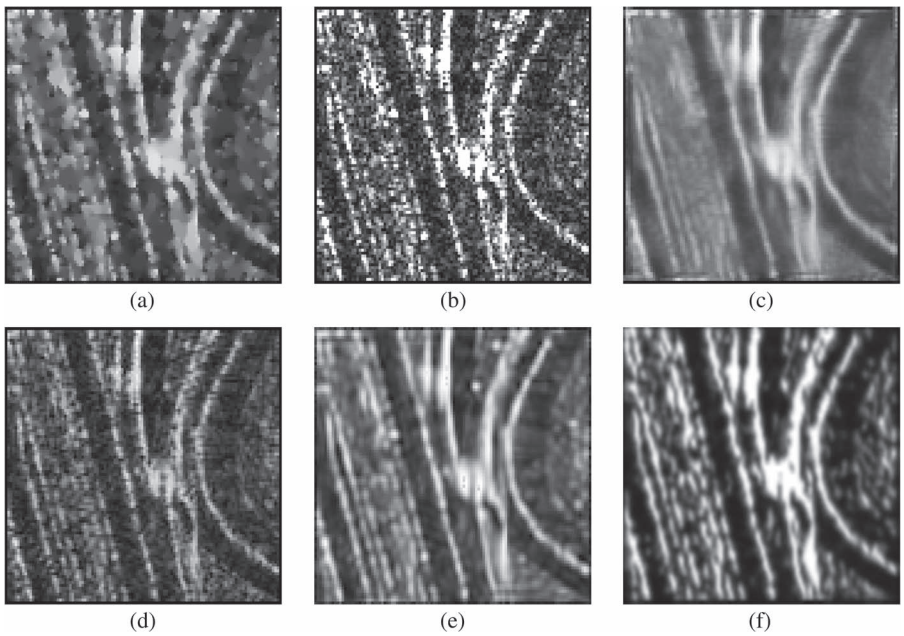

Fig. 8. Zoom of TerraSAR-X SSC image (126 × 116 pixels) of the roads located at the SE of the Macdonald-Cartier Freeway/Allen Road interchange, Toronto, ON, Canada, with $L = 1$. (a) SRAD. (b) Original image. (c) PPB. (d) LPG-PCA. (e) SAR-BM3D. (f) Proposed method.

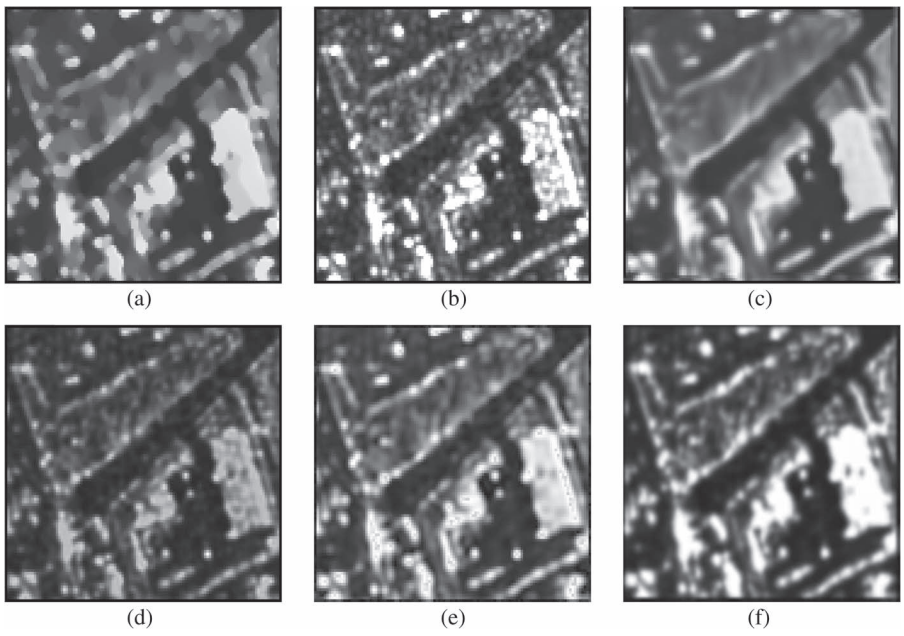

Fig. 9. Zoom of TerraSAR-X MGD SE image (104 × 101 pixels) of the area located at 1077 Wilson Avenue, Toronto, ON, Canada, with $L = 2.1$. (a) SRAD. (b) Original image. (c) PPB. (d) LPG-PCA. (e) SAR-BM3D. (f) Proposed method.

We have tested our denoising scheme in both real and simulated SAR images with several other state-of-the-art methods. The results suggested that our method compared favorably w.r.t. the referenced methods in terms of both image detail preservation and speckle noise reduction.

ACKNOWLEDGMENT

The authors would like to thank the anonymous reviewers whose thorough feedback and suggestions have significantly contributed in improving the quality of this paper and C.-A. Deledalle from the Institut de Mathématiques de Bordeaux, Université Bordeaux, L. Zhang from Hong Kong Polytechnic University, and S. Parrilli from the University of Naples Federico II for making their SAR image denoising codes publically available.

REFERENCES

[1] J. S. Lee, "Digital image enhancement and noise filtering by use of local statistics," *IEEE Pattern Anal. Mach. Intell.*, vol. PAMI-2, no. 3, pp. 165–168, Mar. 1980.

[2] V. S. Frost, J. A. Stiles, K. S. Shanmugan, and J. C. Holtzman, "A model for radar images and its application to adaptive digital filtering of multiplicative noise," *IEEE Trans. Pattern Anal. Mach. Intell.*, vol. PAMI-4, no. 1, pp. 157–166, Mar. 1982.

[3] D. T. Kuan, A. A. Sawchuk, T. C. Strand, and P. Chavel, "Adaptive noise smoothing filter for images with signal-dependent noise," *IEEE Trans. Pattern Anal. Mach. Intell.*, vol. PAMI-7, no. 2, pp. 165–177, Mar. 1985.
[4] Y. Yu and S. T. Acton, "Speckle reducing anisotropic diffusion," *IEEE Trans. Image Process.*, vol. 11, no. 11, pp. 1260–1270, Nov. 2002.
[5] A. Lopes, E. Nezry, R. Touzi, and H. Laur, "Maximum *a posteriori* speckle filtering and first order texture models in SAR images," in *Proc. IEEE Int. Geosci. Remote Sens. Symp.*, 1990, vol. 3, pp. 2409–2412.
[6] L. Gagnon and A. Jouan, "Speckle filtering of SAR images—A comparative study between complex-wavelet-based and standard filters," in *Proc. SPIE*, 1997, pp. 80–91.
[7] H. Guo, J. E. Odegard, M. Lang, R. A. Gopinath, I. W. Selesnick, and C. S. Burrus, "Wavelet based speckle reduction with application to SAR based ATD/R," in *Proc. ICIP*, 1994, pp. 75–79.
[8] A. Achim, P. Tsakalides, and A. Bezarianos, "SAR image denoising via Bayesian wavelet shrinkage based on heavy-tailed modeling," *IEEE Trans. Geosci. Remote Sens.*, vol. 41, no. 8, pp. 1773–1784, Aug. 2003.
[9] S. Solbø and T. Eltoft, "Homomorphic wavelet-based statistical despeckling of SAR images," *IEEE Trans. Geosci. Remote Sens.*, vol. 42, no. 4, pp. 711–721, Apr. 2004.
[10] M. Bhuiyan, M. Ahmad, and M. Swamy, "Spatially adaptive wavelet based method using the cauchy prior for denoising the SAR images," *IEEE Trans. Circuits Syst. Video Technol.*, vol. 17, no. 4, pp. 500–507, Apr. 2007.
[11] F. Argenti and L. Alparone, "Speckle removal from SAR images in the undecimated wavelet domain," *IEEE Trans. Geosci. Remote Sens.*, vol. 40, no. 11, pp. 2363–2374, Nov. 2002.
[12] H. Xie, L. Pierce, and F. Ulaby, "Despeckling SAR images using a low complexity wavelet denoising process," in *Proc. IEEE Int. Geosci. Remote Sens. Symp.*, Nov. 2002, vol. 1, pp. 321–324.
[13] F. Argenti, T. Bianchi, and A. Alparone, "Multiresolution MAP despeckling of SAR images based on locally adaptive generalized Gaussian pdf modeling," *IEEE Trans. Image Process.*, vol. 15, no. 11, pp. 3385–3399, Nov. 2006.
[14] F. Argenti, T. Bianchi, and A. Alparone, "Segmentation-based MAP despeckling of SAR images in the undecimated wavelet domain," *IEEE Trans. Geosci. Remote Sens.*, vol. 46, no. 9, pp. 2728–2742, Sep. 2008.
[15] D. D. Muresan and T. W. Parks, "Adaptive principal components and image denoising," in *Proc. Int. Conf. Image Process.*, 2003, vol. 1, pp. 101–104.
[16] L. Zhang, W. Dong, D. Zhang, and G. Shi, "Two-stage image denoising by principal component analysis with local pixel grouping," *Pattern Recog.*, vol. 43, no. 4, pp. 1531–1549, Apr. 2010.
[17] Y. He, T. Gan, W. Chen, and H. Wang, "Adaptive denoising by singular value decomposition," *IEEE Signal Process. Lett.*, vol. 18, no. 4, pp. 215–218, Apr. 2011.
[18] A. Buades, B. Coll, and J. M. Morel, "A review of image denoising algorithms, with a new one," *Multiscale Model. Simul.*, vol. 4, no. 2, pp. 490–530, Jul. 2005.
[19] P. Coupé, P. Hellier, C. Kervrann, and C. Barillot, "Bayesian non local means-based speckle filtering," in *Proc. 5th IEEE Int. Symp. Biomed. Imaging*, May 2008, pp. 1291–1294.
[20] H. Zhong, J. Xu, and L. Jiao, "Classification based nonlocal means de-speckling for SAR image," in *Proc. SPIE*, 2009, vol. 7495, pp. 74950V-1–74950V-8.
[21] C. Deledalle, L. Denis, and F. Tupin, "Iterative weighted maximum likelihood denoising with probabilistic patch-based weights," *IEEE Trans. Image Process.*, vol. 18, no. 12, pp. 2661–2672, Dec. 2009.
[22] K. Dabov, A. Foi, V. Katkovnik, and K. Egiazarian, "Image denoising by sparse 3D transform-domain collaborative filtering," *IEEE Trans. Image Process.*, vol. 16, no. 8, pp. 2080–2095, Aug. 2007.
[23] J. S. Liu, J. L. Zhang, M. L. Palumbo, and C. E. Lawrence, "Bayesian clustering with variable and transformation selections," in *Bayesian Statistics 7*, J. M. Bernardo, M. J. Bayarri, J. O. Berger, A. P. Dawid, D. Heckerman, A. F. M. Smith, and M. West, Eds. London, U.K.: Oxford Univ. Press, 2003, pp. 249–275.
[24] Y. Liu, W. Li, and Y. Li, "Network traffic classification using K-means clustering," in *Proc. 2nd IMSCCS*, 2007, pp. 360–365.
[25] J. Rissanen, "Modeling by shortest data description," *Automatica*, vol. 14, no. 5, pp. 465–471, Sep. 1978.
[26] M. Wax and T. Kailath, "Detection of signals by information theoretic criteria," *IEEE Trans. Acoust., Speech, Signal Process.*, vol. 33, no. 2, pp. 387–392, Apr. 1985.
[27] S. Lloyd, "Least squares quantization in PCM," *IEEE Trans. Inf. Theory*, vol. 28, no. 2, pp. 129–137, Mar. 1982.
[28] C. Ding and X. He, "K-means clustering via principal component analysis," in *Proc. ICML*, Jul. 2004, pp. 225–232.
[29] F. Sattar, L. Floreby, G. Salomonsson, and B. Lövström, "Image enhancement based on a nonlinear multiscale method," *IEEE Trans. Image Process.*, vol. 6, no. 6, pp. 888–895, Jun. 1997.
[30] S. Parrilli, M. Poderico, C. V. Angelino, and L. Verdoliva, "A nonlocal SAR image denoising algorithm based on LLMMSE wavelet shrinkage," *IEEE Trans. Geosci. Remote Sens.*, vol. 50, no. 2, pp. 606–616, Feb. 2012.

Linlin Xu (S'12) received the B.Eng. and M.Sc. degrees in geomatics engineering from China University of Geosciences, Beijing, China, in 2007 and 2010, respectively. He is currently working toward the Ph.D. degree with a specialization on remote sensing in the Department of Geography and Environmental Management, University of Waterloo, Waterloo, ON, Canada.

His current research interests are in the areas of synthetic aperture radar image processing, segmentation, and classification.

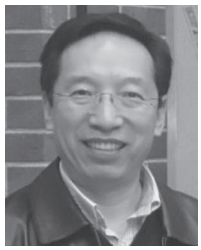

Jonathan Li (M'00–SM'11) received the Ph.D. degree in geomatics engineering from the University of Cape Town, Cape Town, South Africa, in 2000.

He has been with the Key Laboratory of Underwater Acoustic Communication and Marine Information Technology, Xiamen University, Ministry of Education, Beijing, China, since 2011 and a Professor with the Department of Geography and Environmental Management, University of Waterloo, Waterloo, ON, Canada. He has published more than 180 papers in refereed journals, books, and proceedings and has coedited 6 books and 6 theme issues. His current research interests are in the areas of remote sensing of inland and coastal waters, renewable energy potential, and critical infrastructure.

Dr. Li received the 2011 Talbert Abrams Award for best paper in photogrammetry and remote sensing, the 2008 ESRI Award for best paper in GIScience, and the 2006 MDA Award for best paper in photogrammetry and hydrography. He is the Chair of ISPRS ICWG on Land-based Mobile Mapping Systems (2008–2012), Vice Chair of ICA Committee on Mapping from Remote Sensor Imagery (2011–2015), and Vice Chair of FIG Commission on Hydrography (2011–2014).

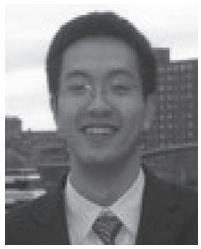

Yuanming Shu received the B.Sc. degree in geography from Nanjing University, Nanjing, China, in 2008 and the M.Sc. degree in geography from the University of Waterloo, Waterloo, ON, Canada, in 2010, where he is currently working toward the Ph.D. degree in the Department of Geography and Environmental Management.

His current research interests are in the areas of object recognition and segmentation of remote sensing images and its associated applications in environmental monitoring.

Mr. Shu was a recipient of the 2010 Canadian Remote Sensing Society Award for Best Master's Thesis.

Junhuan Peng received the Ph.D. degree in geodesy from Wuhan University, Wuhan, China, in 2000.

He is a Professor with the School of Land Science and Techniques, China University of Geosciences, Beijing, China. His current research interests are in the areas of spatial statistics, robust estimation and their associated application in surveying engineering, GPS-based ionosphere analysis, and hydrology data processing.